TREM-2 promotes macrophage survival and lung disease after respiratory viral infection

Kangyun Wu,[1] Derek E. Byers,[1] Xiaohua Jin,[1] Eugene Agapov,[1] Jennifer Alexander-Brett,[1] Anand C. Patel,[1,2] Marina Cella,[3] Susan Gilfilan,[3] Marco Colonna,[3] Daniel L. Kober,[1] Tom J. Brett,[1,4,5] and Michael J. Holtzman[1,5]

[1]Pulmonary and Critical Care Medicine, Department of Medicine, [2]Department of Pediatrics, [3]Department of Pathology and Immunology, [4]Department of Biochemistry and Biophysics, and [5]Department of Cell Biology, Washington University School of Medicine, St. Louis, MO 63110

Viral infections and type 2 immune responses are thought to be critical for the development of chronic respiratory disease, but the link between these events needs to be better defined. Here, we study a mouse model in which infection with a mouse parainfluenza virus known as Sendai virus (SeV) leads to long-term activation of innate immune cells that drive IL-13–dependent lung disease. We find that chronic postviral disease (signified by formation of excess airway mucus and accumulation of M2-differentiating lung macrophages) requires macrophage expression of triggering receptor expressed on myeloid cells-2 (TREM-2). Analysis of mechanism shows that viral replication increases lung macrophage levels of intracellular and cell surface TREM-2, and this action prevents macrophage apoptosis that would otherwise occur during the acute illness (5–12 d after inoculation). However, the largest increases in TREM-2 levels are found as the soluble form (sTREM-2) long after clearance of infection (49 d after inoculation). At this time, IL-13 and the adapter protein DAP12 promote TREM-2 cleavage to sTREM-2 that is unexpectedly active in preventing macrophage apoptosis. The results thereby define an unprecedented mechanism for a feed-forward expansion of lung macrophages (with IL-13 production and consequent M2 differentiation) that further explains how acute infection leads to chronic inflammatory disease.

CORRESPONDENCE
Michael J. Holtzman:
holtzmanm@wustl.edu

Abbreviations used: APEC, airway progenitor epithelial cell; Arg1, arginase 1; Chi3l3, chitinase 3–like-3; COPD, chronic obstructive pulmonary disease; DAP12, DNAX activation protein of 12 kD; dpi, days postinoculation; EpCAM, epithelial cell adhesion molecule; ERK, extracellular signal-regulated kinase; FSC, forward scatter; iNKT cell, invariant NK T cell; MUC5AC, mucin 5AC; Op, osteopetrotic; PKR, protein kinase R; SeV, Sendai virus; SSC, side scatter; sTREM-2, soluble TREM 2; TREM, triggering receptor expressed on myeloid cells.

A critical step toward improved diagnosis and treatment of chronic inflammatory diseases depends on defining the immune mechanisms for the persistent accumulation of activated immune cells in the target tissue. In the case of the lung, clinical evidence suggests that acute infection with a respiratory virus might lead to chronic lung diseases such as asthma and COPD (Holtzman, 2012). To determine precisely how acute infection causes chronic lung disease, we developed a high-fidelity mouse model of this process. In this model, mouse parainfluenza virus (also known as Sendai virus, SeV) is substituted for the related human pathogen to achieve more efficient viral replication and thereby produce the severe acute illness and subsequent chronic respiratory disease that is typical of the pathology found in humans (Walter et al., 2002). Using this model system, we determined that postviral lung disease depends on airway progenitor epithelial cell (APEC) production of IL-33 to drive invariant NK T cells (iNKT cells) and lung

macrophages toward IL-13 production (Kim et al., 2008; Byers et al., 2013). The result is IL-13–dependent inflammation (signified by type 2 activation and accumulation of lung macrophages) and airway mucus production (signified by *MUC5AC* mucin gene expression). This innate epithelial to immune cell loop also appears relevant to human disease because increased numbers of IL-33–expressing APECs are found in association with an IL-13 gene expression signature (including increased MUC5AC mRNA and protein) in the lungs of humans with severe chronic obstructive pulmonary disease (COPD; Kim et al., 2008; Agapov et al., 2009; Alevy et al., 2012; Byers et al., 2013).

In our previous work, we recognized that the APEC population was capable of self-renewal

and inducible release of IL-33 to sustain ongoing activation of the innate immune system (Holtzman et al., 2014). However, the existing data did not explain the selective activation of the lung macrophage population and the special dominance of type 2 (M2) macrophages as a downstream part of the disease process. In the present study, we therefore aimed to better understand how the lung macrophage component of this disease process is triggered by acute infection and then is manifest for months. We reasoned that triggering receptor expressed on myeloid cells 2 (TREM-2) might contribute to this process because M2 polarization is associated with TREM-2 expression in isolated macrophages (Turnbull et al., 2006). In pursuing this possibility, we found that the soluble form of TREM-2 (sTREM-2) was linked to the development of chronic postviral lung disease and was active in promoting macrophage survival. The data stand in contrast to the conventional view that cleavage of cell surface TREM-2 to sTREM-2 results in an inactive end product. The results thereby provide for a previously unrecognized control over macrophage survival and a consequent type 2 immune response that can serve both as a pathogenic mechanism and as a therapeutic target and accompanying biomarker for chronic inflammatory disease.

RESULTS
Macrophage control of postviral disease

To further define the role of macrophages in our postviral mouse model of chronic lung disease (Walter et al., 2002), we first assessed the impact of a new strategy for macrophage deficiency. We previously showed that mice that were treated with clodronate or mice that were homozygous for the *op* mutation in the *Csf1* gene (*Csf1*$^{op/op}$) led to marked macrophage depletion and blockade of postviral lung disease, but both pharmacologic and genetic approaches to depletion led to mice that were also more susceptible to viral infection (Tyner et al., 2005; Kim et al., 2008). In the present case, we started with *Csf1*$^{op/opT}$ (*op/opT*) mice, which carry an osteocalcin-driven *Csf1* transgene (*T*) that rescues the osteopetrotic, but not the macrophage defect, in *op/op* mice (Abboud et al., 2002). We then used these mice to generate heterozygous *Csf1*$^{wt/opT}$ (*wt/opT*) mice with a subtler defect in macrophage level and perhaps function. Of note, we still found that the increase in lung levels of tissue monocytes (SSC^{low}Ly6G$^-$F4/80$^+$CD11b$^+$) and interstitial macrophages (SSC^{high}CD11c$^-$Ly6G$^-$Siglec-F$^-$F4/80$^+$CD11b$^+$) that occurs in WT (*wt/wt*) mice at 5 d post-inoculation (dpi) with Sendai virus (SeV) was significantly attenuated in *wt/opT* mice (Fig. 1 A and Fig. S1). We observed no increase (and instead found a significant decrease) in alveolar macrophages (SSC^{high}CD11c$^+$Ly6G$^-$Siglec-F$^+$F4/80$^+$CD11b$^-$) in *wt/wt* and *wt/opT* mice at 5 dpi, reflecting a predominant effect of Csf1 deficiency on tissue monocytes and interstitial macrophages during acute infection. Despite these differences in lung monocyte–macrophage levels, we found the same degree of acute illness (0–12 dpi) as signified by essentially identical body weight changes, viral titers, and pattern of tissue inflammation in *wt/wt* and *wt/opT* mice (not depicted).

In contrast to the similarities in acute illness in *wt/wt* and *wt/opT* mice, we found marked differences in the development of chronic lung disease that develops after clearance of infectious virus and is fully manifest at 49 dpi (Walter et al., 2002; Kim et al., 2008; Byers et al., 2013). Under these chronic conditions, we observed that the increases in each lung monocyte–macrophage population at 49 dpi in *wt/wt* mice were all markedly attenuated in *wt/opT* mice (Fig. 1 B). Tissue monocytes, which were the most abundant monocyte–macrophage population in the lung, exhibited no increase in *wt/opT* mice at 49 dpi. In concert with the decreased lung monocyte–macrophage levels in *wt/opT* mice, we also found that induction of IL-13 expression and mucous cell metaplasia in *wt/wt* mice was markedly inhibited in *wt/opT* mice at 49 dpi (Fig. 1 C). Similarly, the postviral increases in lung levels of *Il13* mRNA and downstream *Muc5ac* mRNA and type 2 macrophage (M2) markers *Arg1* and *Chitinase 3–like-3 (Chi3l3)* mRNA in *wt/wt* mice were completely blocked in *wt/opT* mice at 49 dpi (Fig. 1 D). These findings are consistent with our previous work showing that lung macrophages are critical for IL-13 production, and in turn, that IL-13 is required to drive mucus production and M2 differentiation in our postviral mouse model of lung disease (Tyner et al., 2006; Kim et al., 2008; Byers et al., 2013). The results also provide a basis for next determining what factors might regulate the expansion of disease-producing lung macrophages under these conditions.

TREM–2 control of postviral disease

Based on the association of TREM-2 with M2 differentiation (Turnbull et al., 2006), we investigated the role of TREM-2 in macrophage-dependent postviral lung disease. In that context, we found that the development of this type of lung disease was associated with increased lung *Trem2* (but not other *Trem*) mRNA levels based on gene expression microarray and real-time qPCR assay (Fig. 2, A and B; and Table S1). Moreover, the development of postviral lung disease at 49 dpi in WT mice was markedly attenuated in *Trem2*$^{-/-}$ mice. Thus, *Trem2*$^{-/-}$ mice showed marked decreases in lung inflammation and airway mucus production based on tissue staining (Fig. 2 C) as well as significantly decreased lung levels of the key cytokine *Il13* mRNA, the predominant mucin *Muc5ac* mRNA, and the M2 markers *Arg1* and *Chi3l3* mRNA based on real-time qPCR assay (Fig. 2 D). *Dap12*$^{-/-}$ mice exhibited a similar inhibition of postviral disease (Fig. 2, C and D), consistent with the association of TREM-2 and DAP12 phenotype in other systems (Bouchon et al., 2000; Kaifu et al., 2003; Turnbull et al., 2006). In contrast, *Trem1/3*$^{-/-}$ mice manifested no significant difference in the development of chronic postviral disease (Fig. 2, C and D), perhaps divergent from the pro-inflammatory role of TREM-1 in other disease models (Bouchon et al., 2001a; Schenk et al., 2007; Klesney-Tait et al., 2013).

The distinct nature of TREM-2 actions in postviral lung disease prompted a further examination of mechanism. We
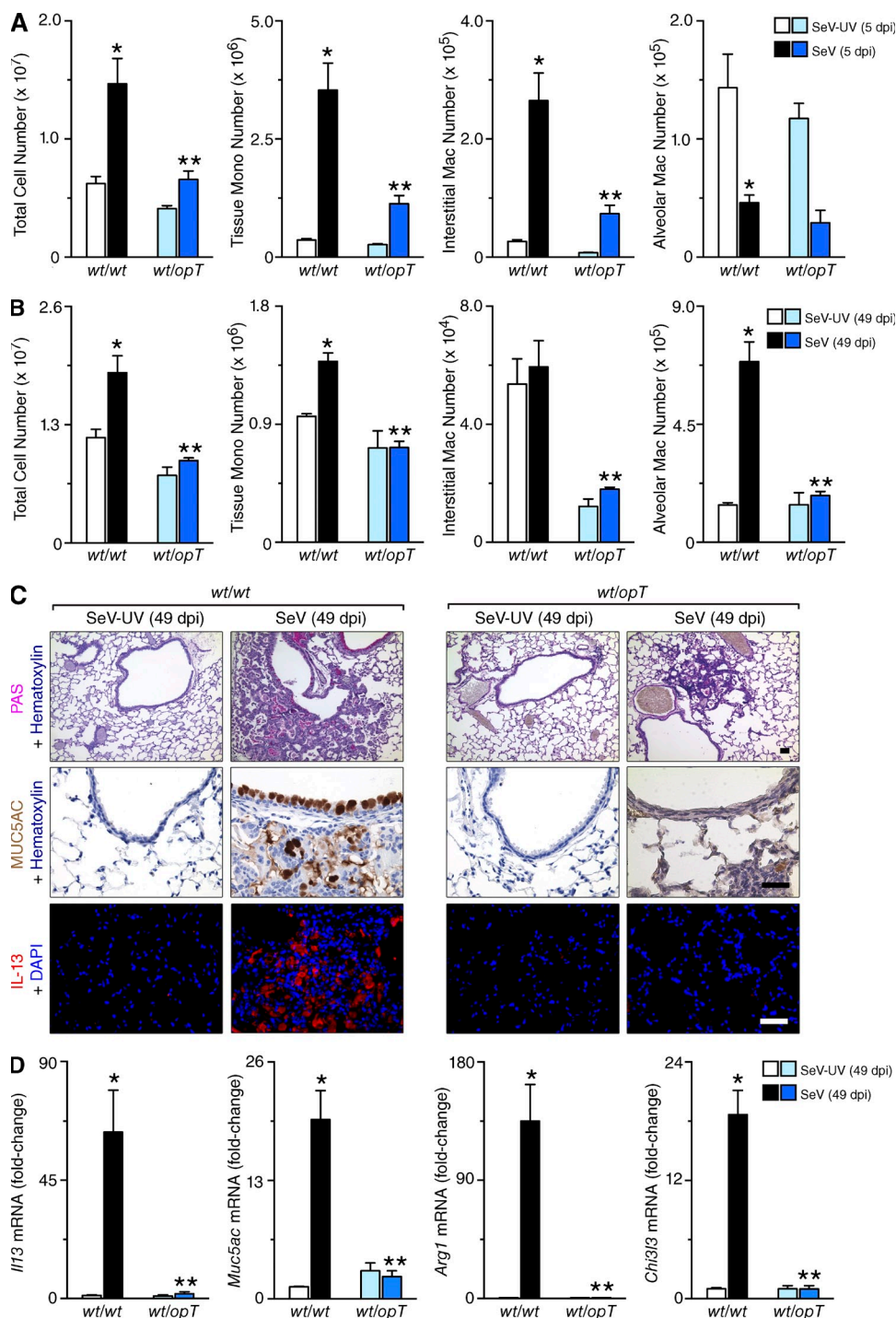
Figure 1. Effect of macrophage deficiency on postviral lung disease. (A) Lung levels of total cells, tissue monocytes (tissue monos), interstitial macrophages (interstitial macs), and alveolar macrophages (alveolar macs) for *wt/wt* and *wt/opT* mice at 5 dpi with SeV or UV-inactivated SeV (SeV-UV) determined by flow cytometry staining with fluorescent bead-based quantitation. (B) For conditions in (A), corresponding values for 49 dpi. (C) Representative photomicrographs of lung sections stained with PAS plus hematoxylin, immunostained for MUC5AC and counterstained with hematoxylin, or immunostained for IL-13 and counterstained with DAPI. Bars, 200 µm. (D) Lung levels of *Il13*, *Muc5ac*, *Arg1*, and *Chi3l3* mRNA in *wt/wt* and *wt/opT* mice at 49 dpi with SeV or SeV-UV. For A, B, and D, * represents a significant increase from SeV-UV, and ** represents a significant decrease from corresponding *wt/wt* control value. All experimental data were verified in at least three independent experiments.
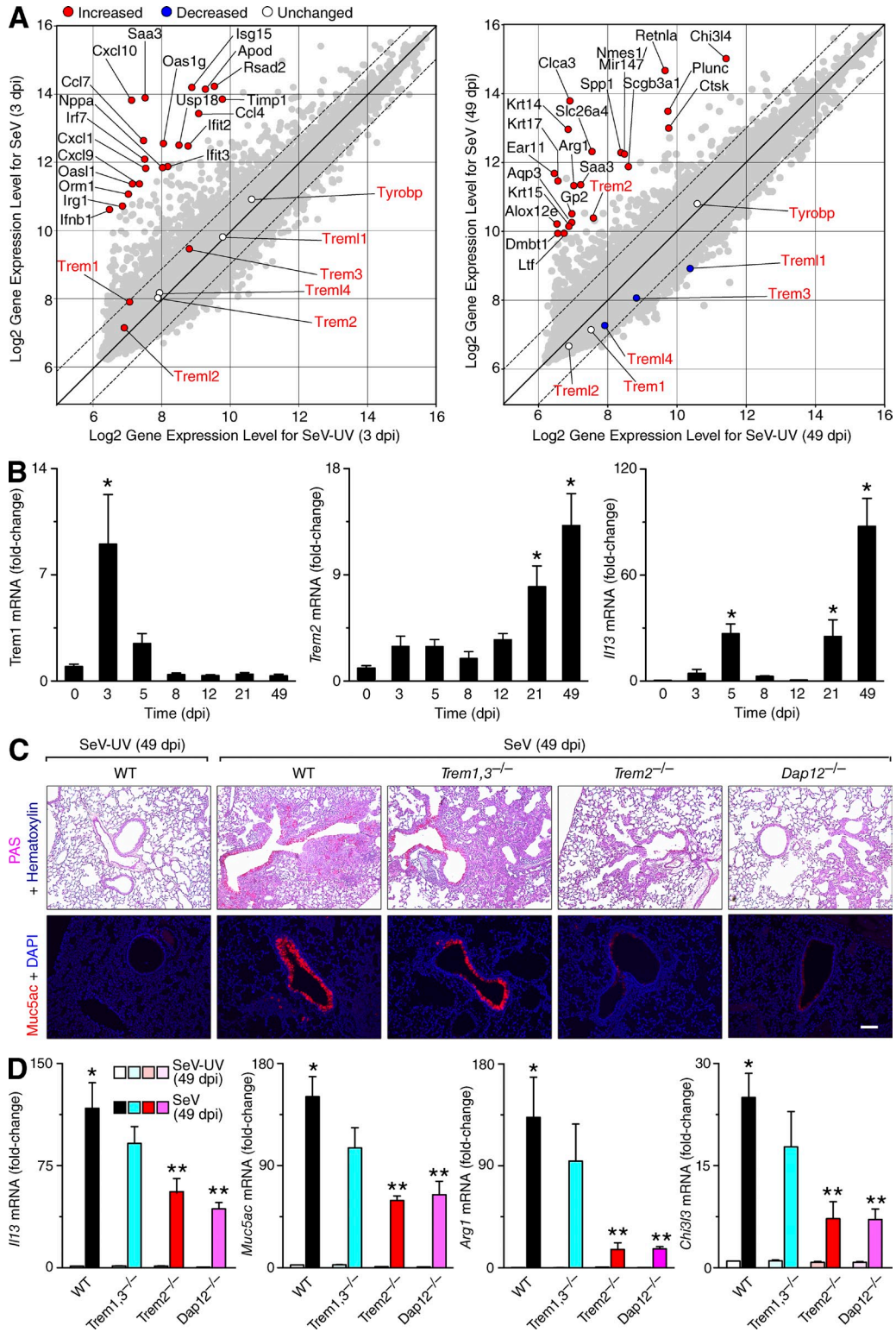
Figure 2. Induction and function of *Trem2* gene expression during postviral lung disease. (A) Gene expression microarray analysis of mRNA from lungs of mice at 3 and 49 dpi with SeV (10⁵ pfu) or SeV-UV. Scatter plot depicts log₂ normalized gene expression. Each symbol represents the expression value for an individual gene with the top 20 differentially expressed genes colored red and annotated in black, and others colored gray. Genes encoding *Trem* family members and *Dap12* are colored red if significantly increased, blue if decreased, or white if unchanged, and are annotated in red. (B) Lung levels of *Trem1*, *Trem2*, and *Il13* mRNA at indicated dpi with SeV. * represents a significant increase from (–) SeV control value. Values at 0 dpi were no different than those for SeV-UV 0–49 dpi. (C) Representative photomicrographs of PAS and Muc5ac staining of lung sections from WT, *Trem2*⁻/⁻,
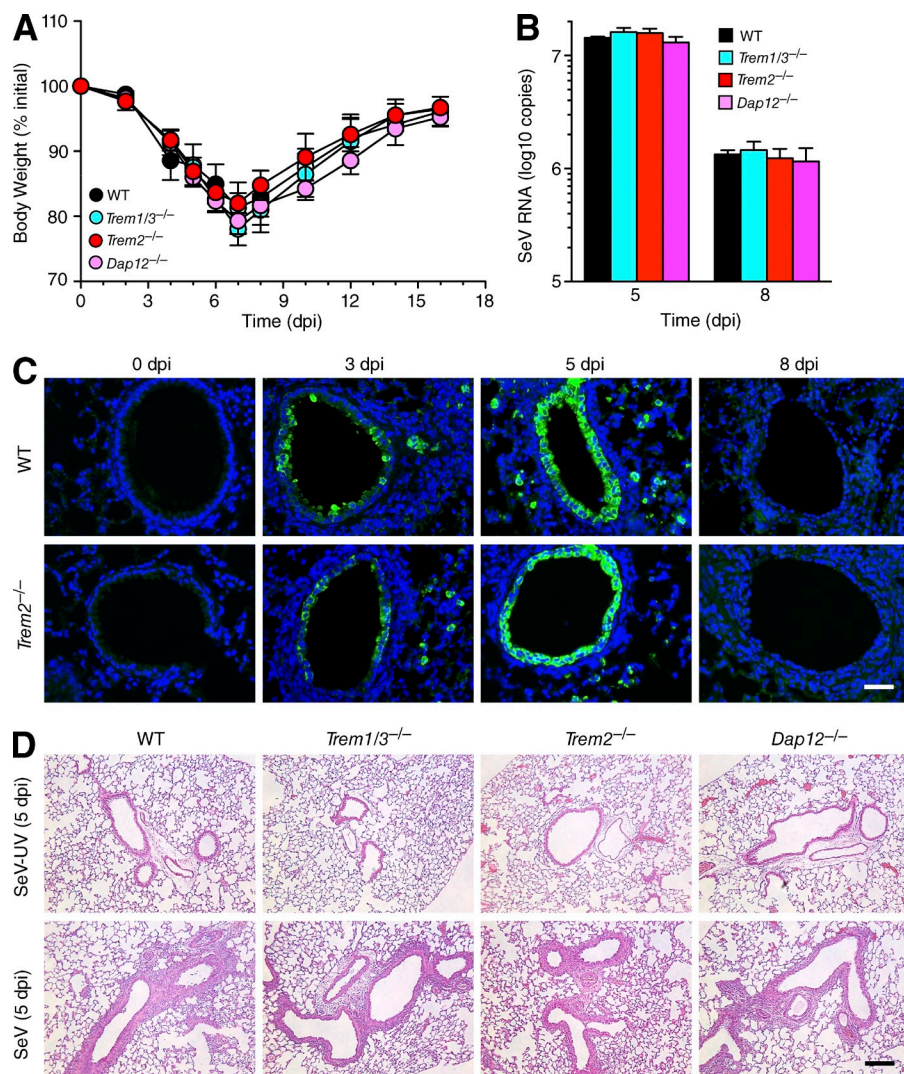
Figure 3. Similarity of acute illness after viral infection in WT and knockout mice. (A) Body weights in WT, *Trem2*$^{-/-}$, *Dap12*$^{-/-}$, and *Trem1/3*$^{-/-}$ mice at the indicated dpi. (B) Viral titers assessed by real-time qPCR assay for SeV N gene RNA in lungs of indicated mouse strains at 5 and 8 dpi. For A and B, values represent mean ± SEM for 4–7 mice. (C) Representative photomicrographs SeV immunostaining in lung sections from WT and *Trem2*$^{-/-}$ mice at 0–8 dpi. (D) Representative photomicrographs of hematoxylin and eosin staining of lung sections from indicated mouse strains at 5 dpi. Each section contains an area of bronchiolitis with inflammatory cells surrounding an airway and adjacent blood vessel. Bar, 200 µm. All experimental data were verified in at least three independent experiments.

first established that there was no significant difference in acute illness among *Trem2*$^{-/-}$, *Dap12*$^{-/-}$, and *Trem1/3*$^{-/-}$ mice as signified by similarities in body weight change, viral titer and tissue distribution, and pattern of tissue inflammation (Fig. 3, A–D). Therefore, we returned to our interest in the role of TREM-2 in modifying long-term macrophage function. We first found that TREM-2 expression at 49 dpi was specific to lung tissue macrophages based on co-localization with macrophage markers F4/80 and Mac-3 in tissue immunostaining (Fig. 4 A). Similarly, TREM-2 expression was found in lung macrophages (CD45$^+$F4/80$^+$) and not stromal cells, e.g., epithelial cells (CD45$^-$EpCAM$^+$), based on flow cytometry staining (unpublished data).

As demonstrated previously (Kim et al., 2008), we also found a marked expansion of IL-13$^+$ lung macrophages in

WT mice at 49 dpi (Fig. 4 B). Here, we show that this expansion is markedly down-regulated in *Trem2*$^{-/-}$ mice based on tissue immunostaining (Fig. 4 B). In addition, FACS-based separation of lung macrophage populations revealed that tissue monocytes and interstitial macrophages exhibited a marked increase in *Il13*, *Arg1*, and *Chi3l3* mRNA levels with the development of postviral disease at 49 dpi in WT mice, and this postviral induction was markedly attenuated in *Trem2*$^{-/-}$ mice (Fig. 4 C). In contrast, alveolar macrophages showed no induction of *Il13* mRNA but nonetheless still manifested a slight increase in *Arg1* mRNA and a marked increase in *Chi3l3* mRNA at 49 dpi in WT mice. The observed levels of *Il13*, *Arg1*, and *Chi3l3* mRNA in alveolar macrophages from WT mice were nearly identical to those in *Trem2*$^{-/-}$ mice (Fig. 4 C). This subset profile might again reflect a predominant

Dap12$^{-/-}$, and *Trem1/3*$^{-/-}$ mice at SeV p.i. day 49. Bar, 200 µm. (D) Corresponding lung levels of *Il13*, *Muc5ac*, *Arg1*, and *Chi3l3* mRNA for conditions in (A). * represents a significant increase from SeV-UV mice and ** a significant decrease from corresponding WT control mice. All experimental data were verified in at least three independent experiments.
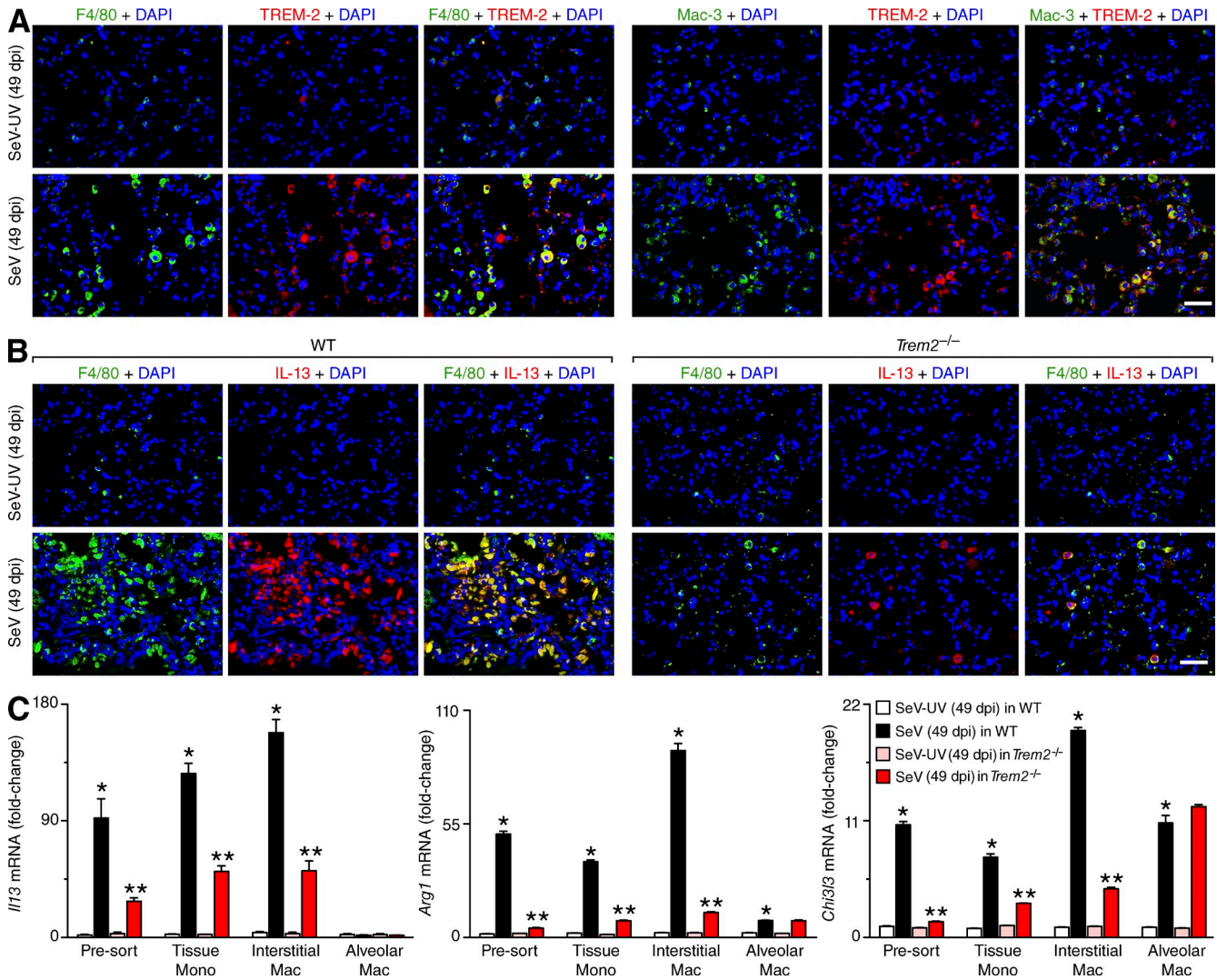
Figure 4. Induction and function of TREM-2 in lung macrophages during postviral lung disease. (A) Representative photomicrographs of TREM-2 plus F4/80 or Mac-3 immunostaining of lung sections from WT mice at 49 dpi with SeV or SeV-UV. Bar, 200 µm. (B) Representative photomicrographs of F4/80 plus IL-13 immunostaining of lung sections from WT and *Trem2⁻/⁻* mice at 49 dpi with SeV-UV or SeV. Bar, 200 µm. (C) Levels of *Il13*, *Arg1*, and *Chi3l3* mRNA in FACS-purified tissue monos, interstitial macs, and alveolar macs from WT and *Trem2⁻/⁻* mice at 49 dpi with SeV or SeV-UV. Each value represents mean ± SEM for five mice and is representative of three experiments. * represents a significant increase from corresponding SeV-UV in WT value, and ** represents a significant decrease from corresponding SeV in WT value. All experimental data were verified in at least three independent experiments.

effect of TREM-2 deficiency on tissue monocytes and interstitial macrophages. Given the predominance of the tissue monocyte population, these findings were consistent with the decrease in whole lung levels of *Il13*, *Arg1*, and *Chi3l3* mRNA found in *Trem2⁻/⁻* mice.

Cell surface TREM-2 expression and function

We next assessed the regulation of TREM-2 expression and function under the current paradigm that TREM-2 expressed on the cell surface works in coordination with its adapter protein DAP12 to signal for macrophage activation (Turnbull et al., 2006). In the present model, cell surface expression of TREM-2 on lung macrophages was detected on tissue monocytes and interstitial macrophages but not alveolar macrophages

(Fig. 5 A). Moreover, flow cytometry staining for TREM-2 was found exclusively on CD11b⁺CD11c⁻ lung cells at 5 dpi (Fig. S2), which is consistent with localization to tissue monocytes and interstitial macrophages and not to alveolar macrophages or dendritic cells. Postviral induction of cell surface TREM-2 was found only at 2–8 dpi (Fig. 5, A and B) and was therefore similar to induction for lung levels of SeV, suggesting that SeV replication might increase cell surface TREM-2 on macrophages. To follow up this possibility, we studied BMDMs infected with GFP-labeled SeV and showed an increase in cell surface staining for TREM-2 that correlated closely with viral titer (Fig. 5, C and D). Moreover, SeV infection caused a dose-dependent increase in cell surface TREM-2 levels on BMDMs that was reproduced using poly(IC) treatment,
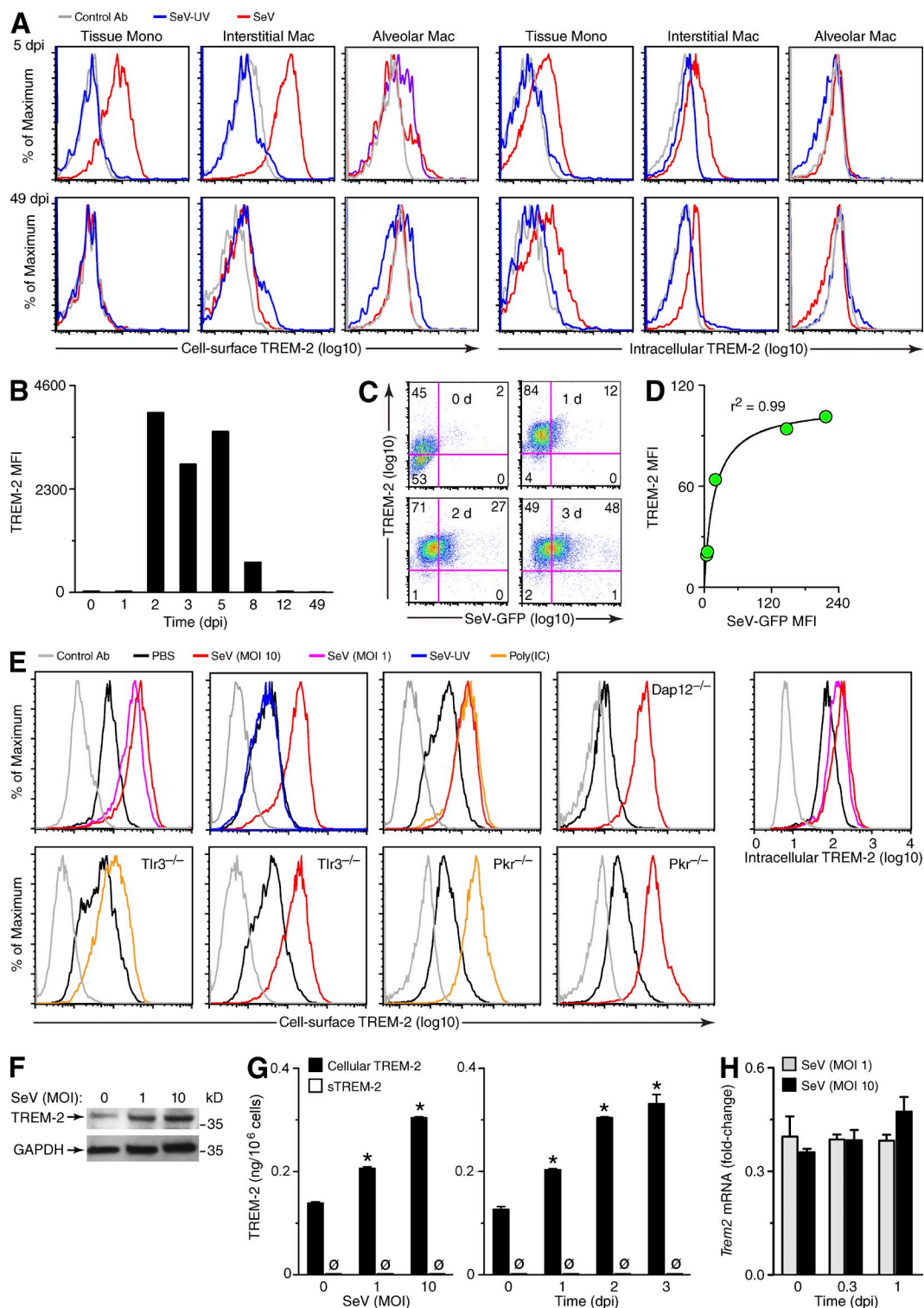
Figure 5. Regulation of cell surface and intracellular TREM-2 levels during viral replication and postviral lung disease. (A) Representative histograms from FACS analysis of TREM-2 immunostaining for tissue monos, interstitial macs, and alveolar macs from lungs of mice at 5 or 49 dpi with SeV-UV or SeV. (B) Corresponding MFI values for cell surface TREM-2 levels on tissue monos at the indicated dpi based on analysis conditions in A. (C) Representative cytograms from flow cytometry analysis of cell surface TREM-2 immunostaining for BMDMs at 0–3 dpi with GFP-expressing SeV (SeV-GFP). (D) Corresponding MFI values for cell surface TREM-2 and SeV-GFP for conditions in C. (E) Representative histograms for flow cytometry analysis of cell surface and intracellular TREM-2 immunostaining for BMDMs with indicated conditions. (F) Western blotting of TREM-2 in BMDMs at 2 dpi with SeV (MOI 0–10). (G) ELISA of cellular TREM-2 and sTREM-2 in BMDMs at 2 dpi with SeV for indicated MOI or with SeV at MOI 10 for 0–3 dpi. * represents a significant increase from corresponding control at MOI 0 and 0 dpi and Ø represents an undetectable level of sTREM-2. (H) *Trem2* mRNA level in BMDMs with SeV at MOI 1 and 10 for 0–1 dpi. All experimental data verified in at least three independent experiments.

and this increase was unaffected by DAP12, TLR3, or PKR deficiency (Fig. 5 E). In addition to the increase in surface TREM-2 levels, we also found that SeV infection caused a smaller but sustained increase in intracellular levels of TREM-2 in BM-derived macrophages (BMDMs) unaccompanied by any detectable production of sTREM-2 or any increases in *Trem2* mRNA (Fig. 5, F–H). A similar increase in intracellular TREM-2 level was found in vivo at 5 and 49 dpi. Together, the results suggest that SeV promotes an increase in surface TREM-2 levels based on increased TREM-2 formation and either transport to or retention at the cell surface with relatively little if any TREM-2 cleavage from the cell surface.

The relatively transient increase in cell surface TREM-2 levels suggested an acute effect on macrophage function after viral infection. Consistent with this idea, we found that the increase in the number of tissue monocytes (and interstitial macrophages but not neutrophils) at 5 dpi in WT mice was attenuated in *Trem2*$^{-/-}$ mice (Fig. 6 A and not depicted). This attenuation was not accompanied by decreases in monocyte chemokine production based on lung levels of *Ccl2* and *Cx3cl1* mRNA at 3–5 dpi (Fig. 6 B) or decreases in monocyte influx into the lung based on tracking CD45.2 transferred monocytes by flow cytometry at 5 dpi (Fig. 6 C). However, we did detect increased macrophage apoptosis in *Trem2*$^{-/-}$ mice compared with WT mice based on immunostaining for active caspase-3 and Mac-3 at 5–12 dpi (Fig. 6, D and E), suggesting a role for TREM-2 in specifically promoting macrophage survival after viral infection. Cells that were active caspase-3$^+$ were not also SeV$^+$ (Fig. 6 F), suggesting that TREM-2 antiapoptotic actions were independent of viral cytopathic effect. In addition, the timing of apoptosis corresponded to a relative decrease in *Csf1* mRNA and CSF-1 protein levels in the lung (Fig. 6, G and H), consistent with the link between CSF-1 and macrophage survival via DAP12 signaling (Otero et al., 2009). Moreover, we detected no defect in CSF-1 production in *Trem2*$^{-/-}$ mice suggesting that the CSF-1 survival signal required downstream activation of TREM-2 to prevent apoptosis. Indeed, we found a marked increase in apoptosis with CSF-1 withdrawal in BMDMs from *Trem2*$^{-/-}$ mice compared with WT control mice based on propidium iodide staining, Annexin V staining, and active Caspase-3 immunoblotting (Fig. 6, I–K). We detected a slight increase in apoptosis in BMDMs from *Trem2*$^{-/-}$ mice even in cultures with CSF-1, but this effect was also attributable to CSF-1 withdrawal because CSF-1 was added only once at the start of the 2-d culture period and was therefore being consumed and depleted from the culture medium. This condition therefore represents a partial degree of CSF-1 withdrawal and a consequent loss of the CSF-1 to TREM-2 survival signal in *Trem2*$^{-/-}$ cells. Together, our results suggested that cell surface TREM-2 might preserve macrophage survival and promote macrophage accumulation after viral infection and thereby lead to long-term macrophage-dependent disease. However, the relatively transient effect of TREM-2 during acute infection also raised the possibility that TREM-2 had additional effects at later time points that influenced long-term disease outcome.

sTREM-2 expression and function

To pursue the possible chronic actions of TREM-2 in the postviral model, we first determined whether there was long-term production of TREM-2 protein in the lung in this model. Indeed, we found a marked increase in lung levels of TREM-2 at 49 dpi compared with baseline or to the relatively small increase found at 5 dpi (Fig. 7 A). Given the absence of detectable cell surface TREM-2 at 49 dpi and the relatively small increase in intracellular TREM-2 at either 5 or 49 dpi (Fig. 5 A), this late increase in TREM-2 levels at 49 dpi was likely a marker of sTREM-2 formation in the diseased lung. Since IL-13 production was also markedly increased at 49 dpi, we questioned whether IL-13 might promote TREM-2 cleavage at the cell surface and consequent formation of sTREM-2. In support of this possibility, we found that IL-13 administration caused a time-dependent loss of cell surface levels of TREM-2 in BMDMs (Fig. 7 B). The effect of IL-13 was specific for the IL-13 receptor since the same effect was found for IL-4 (that also activates this receptor) but was not detectable for other type 2 cytokines (IL-5 and IL-9; Fig. 7 C). Treatment with IL-13 also resulted in a time-dependent increase in cellular TREM-2 levels in BMDMs, as expected for M2 differentiation, but caused an even greater increase in sTREM-2 levels released from BMDMs (Fig. 7 D). The increases in cellular TREM-2, especially the even greater increases in sTREM-2 production, were attenuated in BMDMs from *Dap12*$^{-/-}$ mice (Fig. 7 D). Moreover, the expected increase in sTREM-2 levels was not found during postviral disease in *Dap12*$^{-/-}$ mice (Fig. 7 E). Together, these findings indicated that both IL-13 and DAP12 were contributing to sTREM-2 formation and any consequent function of sTREM-2 in chronic postviral disease.

To pursue a possible role for sTREM-2 in postviral disease, we analyzed the effect of recombinant sTREM-2 (amino acids 19–136) on macrophage function. Immunostaining of BMDMs incubated with sTREM-2 showed that the protein was localized to the cell cytoplasm and not the cell surface and was thereby accessible to intracellular proteins (Fig. 8 A). In that context, we found that sTREM-2 administration to BMDMs caused a significant increase in *Arg1* mRNA levels (as a sign of M2 differentiation), but the increase was not preserved for other M2 markers (e.g., *Chi3l3* mRNA) and was not nearly as effective as IL-13 for driving these responses (Fig. 8 B). Thus, the direct effect of sTREM-2 on M2 differentiation was relatively small and was therefore unlikely to contribute to biological function or postviral disease. However, in the process of conducting these experiments, we recognized that sTREM-2 treatment of BMDMs resulted in marked protection against the usual progression to cell death in this culture system, and this protective effect resulted in expanded numbers of BMDMs from both WT and *Trem2*$^{-/-}$ mice (Fig. 8 C). Similarly, sTREM-2 treatment caused a dose-dependent expansion of BMDMs from WT, *Trem2*$^{-/-}$, and *Dap12*$^{-/-}$ mice (Fig. 8 D). Here again,
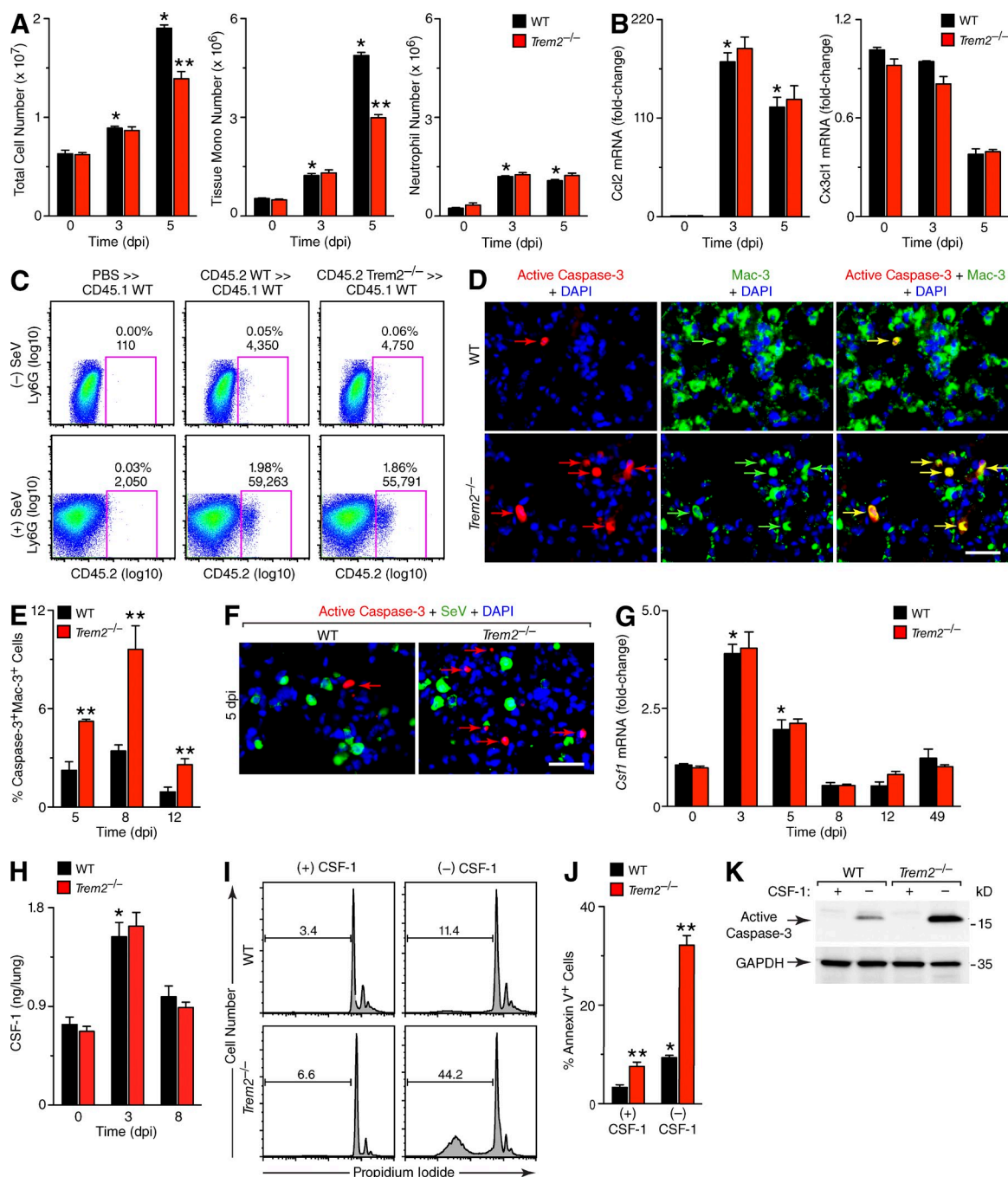
Figure 6. Effect of cellular TREM-2 on macrophage apoptosis during acute viral infection. (A) Flow cytometry analysis of lung levels of total cells, tissue monos, and neutrophils (SSC^highLy6G^+) for WT and *Trem2^−/−* mice at 0–5 dpi with SeV. (B) *Ccl2* and *Cx3cl1* mRNA levels in WT and *Trem2^−/−* mice at 0–5 dpi. For A and B, values represent mean ± SEM for 5 mice, and * represents a significant increase from 0 dpi and ** a significant decrease from corresponding WT mice. (C) Representative cytograms for flow cytometry analysis of levels of CD45.2^+ tissue monos in WT and *Trem2^−/−* mice at 3 dpi after CD45.2 WT and *Trem2^−/−* BMDMs were introduced into CD45.1 WT mice at 0 dpi. (D) Representative photomicrographs of active caspase-3 and Mac-3 immunostaining of lung sections from WT and *Trem2^−/−* mice at 8 dpi. Arrows indicate cells with double-positive immunostaining. Bar, 200 µm. (E) Quantification of analysis in (D). Values represent mean ± SEM for 12 randomly selected fields of lung sections from 3 mice, and ** represents a significant increase from corresponding WT mice. (F) Representative photomicrographs of active caspase-3 and SeV immunostaining of lung sections from WT and *Trem2^−/−* mice at 5 dpi. Arrows indicate cells with active caspase-3^+ immunostaining. Bar, 200 µm. (G) Lung levels of *Csf1* mRNA for WT and *Trem2^−/−* mice at indicated dpi. (H) Corresponding lung levels of CSF-1 for conditions in (G). For G and H, values represent mean ± SEM for 5 mice, and * represents a significant increase from 0 dpi. (I) Flow cytometry analysis of propidium iodide staining of BMDMs from WT and *Trem2^−/−* mice cultured with or without CSF-1 for 1 d. (J) Levels of Annexin V immunostaining in PI^− cells for culture conditions in (I). Values represent mean ± SEM for 6 randomly selected fields of replicate wells, and * represents a significant increase from (+) CSF-1, and ** a significant increase from corresponding WT mice. (K) Western blot levels of active caspase-3 for culture conditions in I. All experimental data were verified in at least three independent experiments.
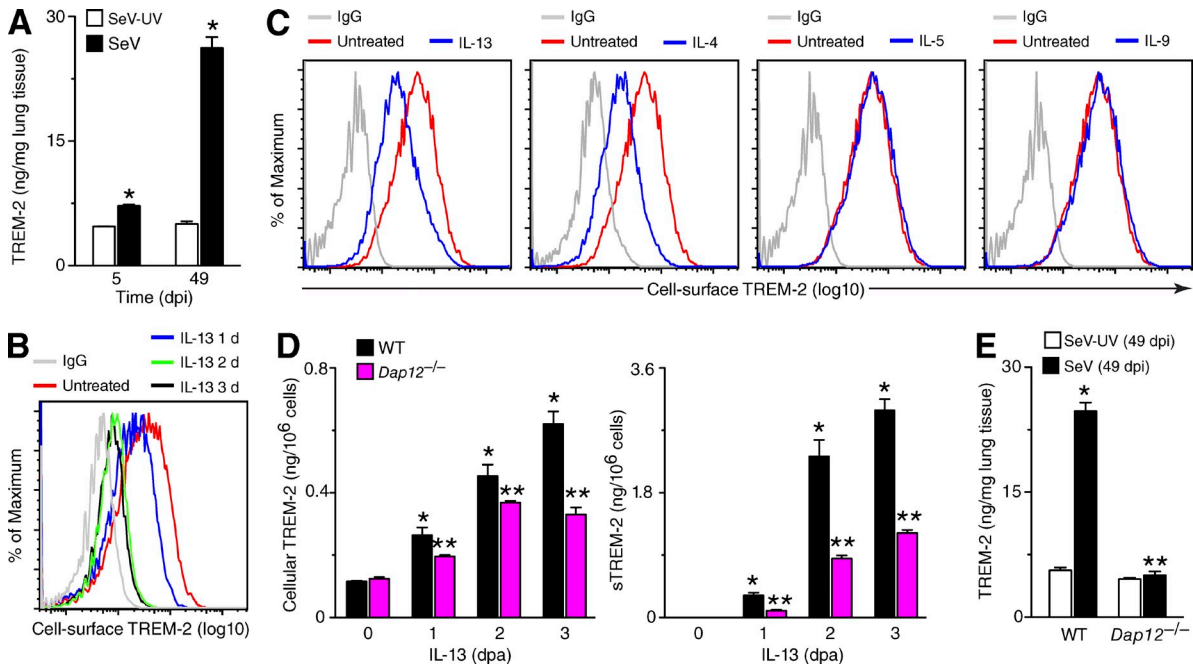
Figure 7. Effect of IL-13 on production of sTREM-2. (A) Lung levels of TREM-2 determined by ELISA at 5 or 49 dpi with SeV or SeV-UV. Values represent mean ± SEM for 5 mice, and * represents a significant increase from corresponding SeV-UV mice. (B) Representative histograms from flow cytometry analysis of cell surface TREM-2 on BMDMs treated with or without IL-13 (20 ng/ml) or IgG control for 1–3 d. (C) Representative histograms from flow cytometry analysis of cell surface TREM-2 on BMDMs treated with or without IL-13, IL-4, IL-5, or IL-9 (20 ng/ml) or IgG control for 1 d. (D) Levels of cellular and sTREM-2 in BMDMs obtained from WT and *Dap12*−/− mice and cultured with IL-13 for 1–3 d post-administration (dpa) as in B. Values represent mean ± SEM for 3 replicate wells, and * represents a significant increase from 0 dpa and ** a significant decrease from corresponding WT cells. (E) Lung levels of TREM-2 in WT and *Dap12*−/− mice at 49 dpi. Values represent mean ± SEM for 5 mice, and * represents a significant increase from SeV-UV and ** a significant decrease from corresponding WT mice. All experimental data were verified in at least three independent experiments.

the baseline numbers of BMDMs were increased in WT mice compared with *Trem2*−/−, and *Dap12*−/− mice under these culture conditions, but this difference was corrected in response to sTREM-2 treatment (Fig. 8 D). The protective effect was specific for active sTREM-2 because it was lost with heat inactivation (Fig. 8 E). Flow cytometry analysis with propidium iodide staining indicated that sTREM-2 administration resulted in attenuation of apoptosis due to CSF-1 withdrawal in BMDMs from WT mice, as well as *Trem2*−/− and *Dap12*−/− mice (Fig. 8 F). As expected, the level of apoptosis with CSF-1 withdrawal in BMDMs from WT mice was markedly increased in *Trem2*−/− and *Dap12*−/− mice, but this effect was also fully preventable and dose-dependent with sTREM-2 administration (Fig. 8 F). Treatment with sTREM-2 also reversed the increase in activate caspase-3 levels that develops with CSF-1 withdrawal, confirming an effect on apoptosis (Fig. 8 G). In contrast, sTREM-2 had no effect on cellular proliferation based on BrdU incorporation (Fig. 8 H), as expected for cell cultures deprived of CSF-1 stimulation. This result is also consistent with the absence of significant cell proliferation in the lung in vivo when disease becomes manifest (Tyner et al., 2006). Together, these findings support a role for sTREM-2 in protection against macrophage apoptosis under low CSF-1 conditions, and thereby explained

the increased levels of apoptosis under these conditions in *Trem2*−/− and *Dap12*−/− macrophages that are unable to generate sTREM-2.

Given the difficulties in monitoring apoptosis in vivo (e.g., we detected no active caspase-3 tissue staining at 49 dpi; unpublished data) we sought additional markers of sTREM-2 action during postviral lung disease. In that regard, we were able to establish that sTREM-2 treatment resulted in a time-dependent and selective increase in molecular pathways connected to cell survival and proliferation, e.g., ERK1/2 and MAPK14 phosphorylation but not AKT phosphorylation or BCL-2 induction (Fig. 9 A). The effect of sTREM-2 on phospho-ERK1/2 and phospho-MAPK formation was more pronounced in BMDMs from *Trem2*−/− mice compared with WT mice (Fig. 9 A), consistent with the enhanced effect of sTREM-2 on viability of BMDMs from *Trem-2*−/− compared with WT mice based on fold-change (Fig. 8 D). In translating these findings to the postviral model in vivo, we found that phospho-ERK1/2 immunostaining was markedly increased and co-localized to lung macrophages at 49 dpi compared with 5 dpi or SeV-UV control conditions in WT mice (Fig. 9 B). Moreover, the increase in phospho-ERK1/2 immunostaining was not detected at 49 dpi in *Trem2*−/− mice (Fig. 9 B). These results were consistent with increases in the numbers of total
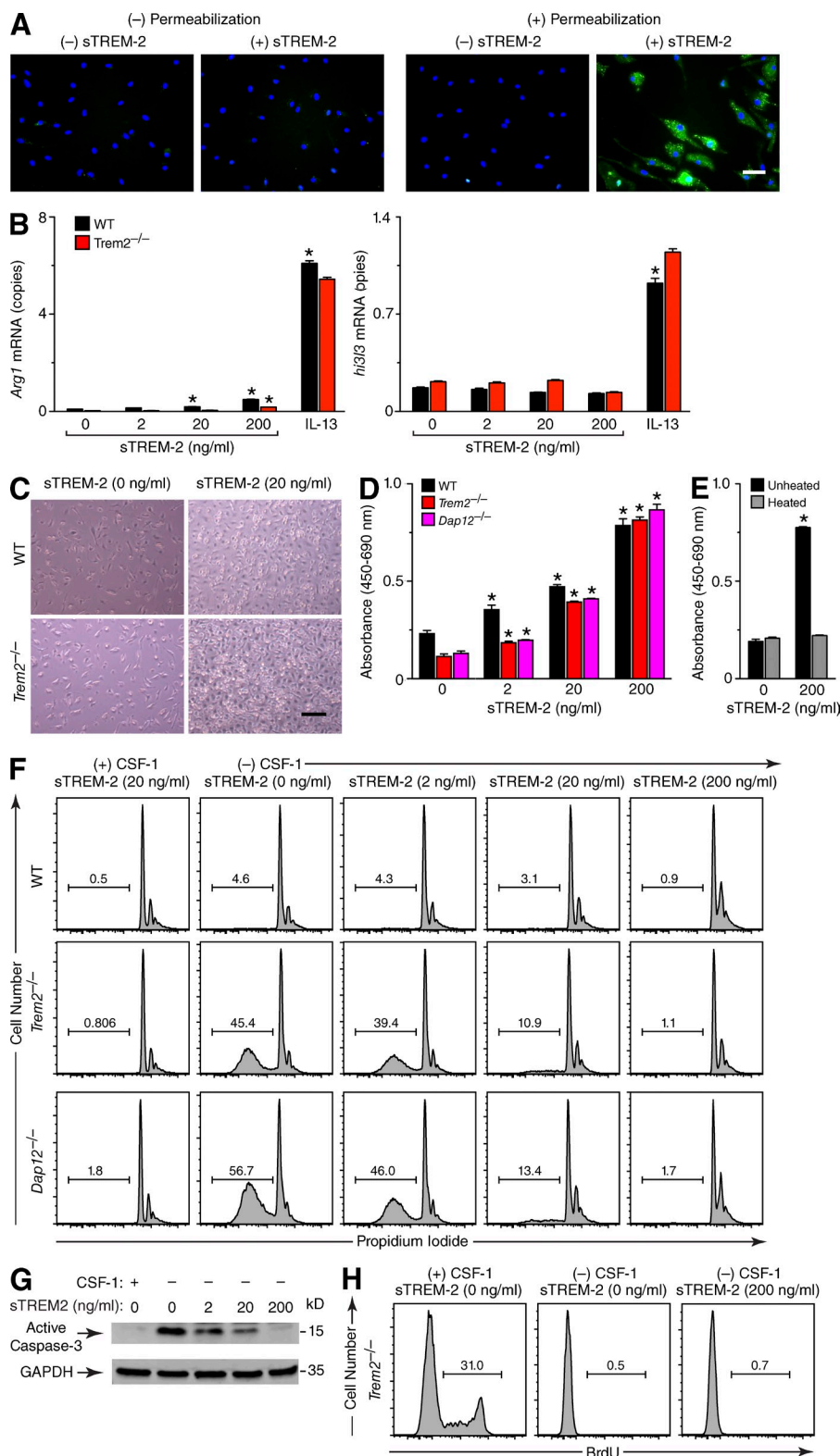
Figure 8. Effect of sTREM-2 on macrophage apoptosis. (A) Representative photomicrographs of immunostaining for recombinant sTREM-2 after incubation with BMDMs for 30 min with and without cell permeabilization with saponin. Bar, 100 µm. (B) Levels of *Arg1* and *Chi3l3* mRNA in BMDMs obtained from *Trem2*−/− and WT mice and then cultured with sTREM-2 (0–200 ng/ml) or IL-13 (20 ng/ml) for 1 d. Values represent mean ± SEM for 3 replicate wells, and * represents a significant increase from no treatment control (0 ng/ml). (C) Representative photomicrographs of sTREM-2–treated BMDMs cultured in 15% L-cell conditioned medium for 7 d. Bar = 200 µm. (D) XTT assay for BMDMs obtained from WT, *Trem2*−/−, and *Dap12*−/− mice and then cultured with sTREM-2 (0–200 ng/ml) for 2 d after CSF-1 withdrawal. Values represent mean ± SEM for 3 replicate wells, and * represents a significant increase from corresponding untreated control cells. (E) XTT assay of BMDMs from WT mice cultured with native (unheated) or denatured (heated) sTREM-2 (0–200 ng/ml) with culture conditions in D. * represents a significant increase from corresponding untreated control cells. (F) Flow cytometry analysis of propidium iodide staining of BMDMs obtained from WT, *Trem2*−/−, and *Dap12*−/− mice and cultured with sTREM-2 (0–200 ng/ml) with or without CSF-1 for 1 d. (G) Western blot levels of active caspase-3 for culture conditions in F. (H) Flow cytometry analysis of BrdU-labeling of BMDMs from *Trem2*−/− mice for culture conditions in F. All experimental data were verified in at least three independent experiments.

immune cells and macrophages in the lung at 49 dpi in WT mice, as well as marked inhibition of this cellular response at 49 dpi in *Trem2*−/− mice (Fig. 9 C). Together, these findings provide for a crucial regulatory role of TREM-2 in a feed-forward pathway that expands the M2 macrophage population and thereby promotes IL-13–dependent chronic lung disease.
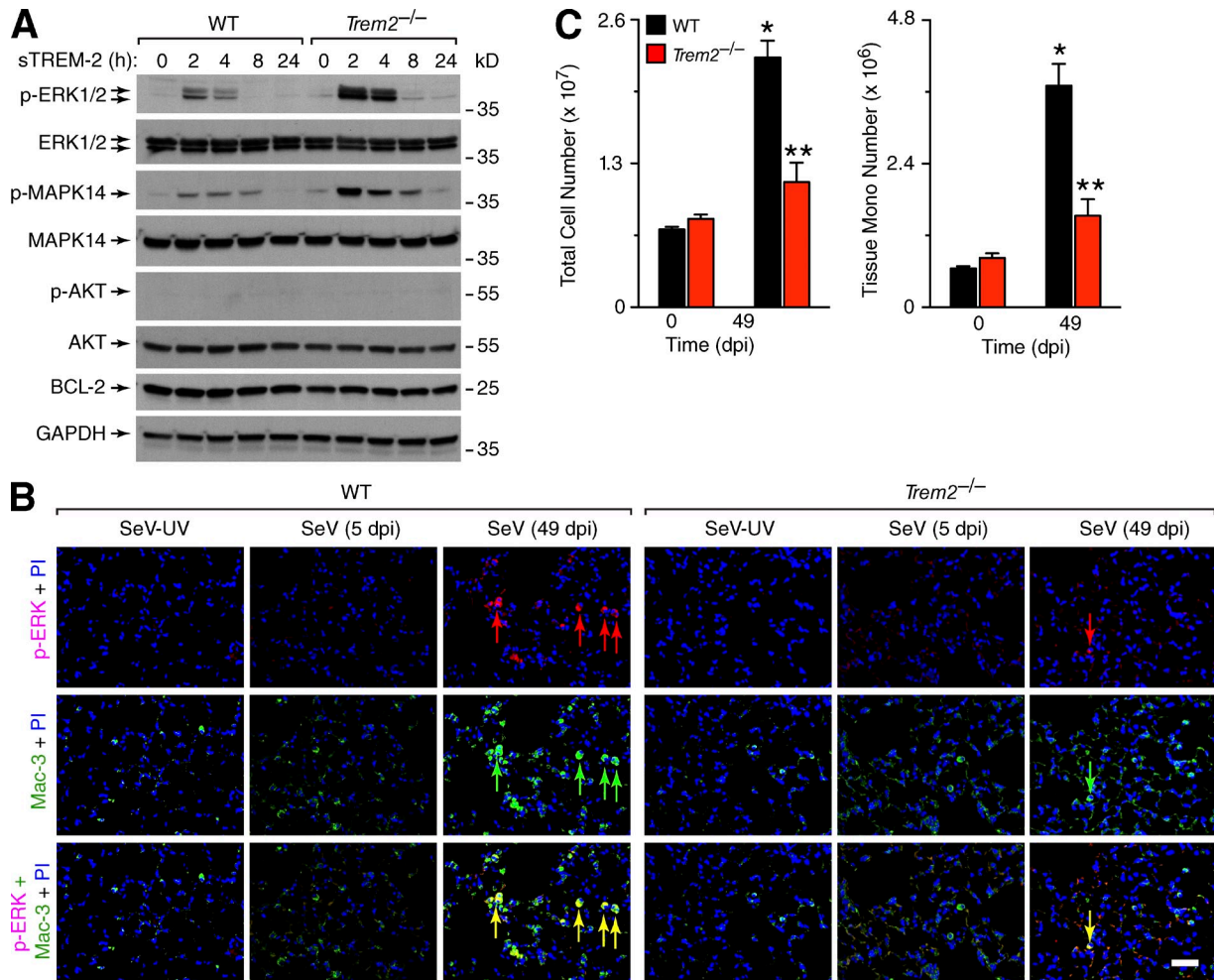
Figure 9. Effect of TREM–2 deficiency on apoptosis signaling pathway. (A) Western blot levels of indicated cell survival proteins in BMDMs cultured from WT and Trem22/2 mice after treatment with mouse sTREM-2 (200 ng/ml) for 0–24 h. (B) Representative photomicrographs of phospho-ERK1/2 (p-ERK) and Mac-3 immunostaining with DAPI counterstaining of lung sections from WT and Trem22/2 mice at 5 or 49 dpi with SeV or SeV-UV. Arrows indicate cells with double-positive immunostaining. Bar, 200 µm. (C) Flow cytometry analysis of lung levels of total cells and tissue monos for WT and Trem22/2 mice at 0 and 49 dpi. Values represent mean ± SEM for 5 mice, and * represents a significant increase from 0 dpi and ** a significant decrease from corresponding WT mice. Values at 0 dpi were no different than those for SeV-UV (49 dpi). All experimental data were verified in at least three independent experiments.

DISCUSSION

This report identifies TREM-2 as a key component of an innate immune pathway for the pathogenesis of chronic lung disease. We use a postviral mouse model of this type of disease to show that: (1) during acute illness, viral replication increases lung macrophage levels of intracellular and cell surface TREM-2, and this action mediates a CSF-1–dependent cell survival signal that prevents macrophage apoptosis; (2) during chronic postviral disease, IL-13 and DAP12 signals promote increased expression and cleavage of TREM-2 from the cell surface to form sTREM-2 at increased levels in the lung; and (3) sTREM-2 is not inactive as previously thought, but is instead capable of promoting macrophage survival via antiapoptotic signals such as ERK1/2 activation. Together, these events allow for TREM-2 to participate in a feed forward mechanism to amplify the accumulation of macrophages

in the lung. In the context of our previous work, the increased number of macrophages would be available to interact with iNKT cells and drive further IL-13 production thereby resulting in IL-13–dependent differentiation of the macrophage population toward an M2 pattern of gene expression (including *Arg1* and *Chi3l3*) and differentiation of an airway progenitor epithelial cell (APEC) niche to airway mucous cells (AMCs) as signatures of chronic lung disease (as diagrammed in Fig. 10). The scheme is consistent with our observation that TREM-2–deficient mice are markedly protected from the development of chronic lung disease as a long-term consequence of viral infection.

The role of TREM-2 in chronic disease described in this study provides for at least four major and unexpected insights. First, TREM-2 signaling was often portrayed as antiinflammatory and reparative, whereas increased TREM-1 signals
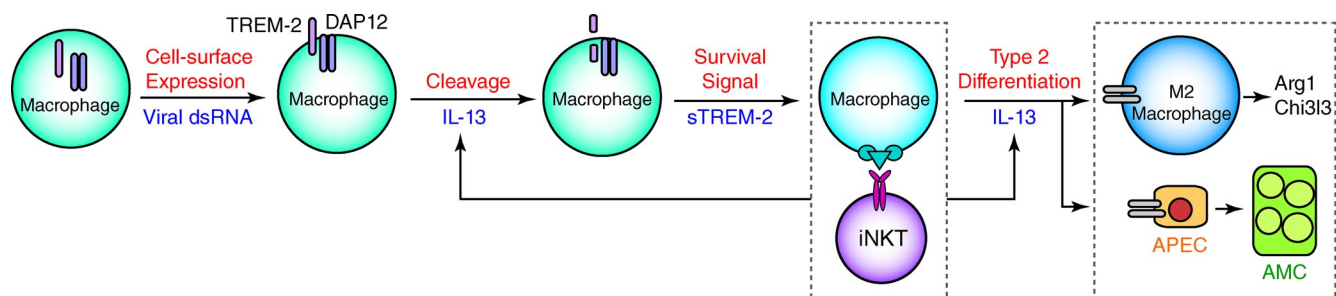
Figure 10. Scheme for regulation and function of TREM–2 in chronic postviral lung disease. Major steps include: (1) early activation of lung macrophages in which viral replication increases TREM-2 at the cell surface; (2) cleavage of TREM-2 from the cell surface to form sTREM-2 in a process that is up-regulated by IL-13 and DAP12; (3) sTREM-2 actions to prevent apoptosis in association with increased ERK1/2 activation and thereby allow for amplified macrophage interaction with iNKT cells and consequent IL-13 production; and (4) IL-13–dependent differentiation of the macrophage population toward an M2 pattern of gene expression (including Arg1 and Chi3l3) and differentiation of an airway progenitor epithelial cell (APEC) niche to airway mucous cells (AMCs) as signatures of chronic lung disease.

were thought to be proinflammatory and destructive in models of intestinal and CNS disease (Schenk et al., 2007; Takahashi et al., 2007; Seno et al., 2009). This view is consistent with studies showing that engagement of TREM-1 promotes secretion of proinflammatory cytokines (including IL-6 and TNF) and increases the inflammatory responses downstream of TLR and NLR engagement (Bouchon et al., 2000, 2001a; Bleharski et al., 2003; Netea et al., 2006; Fortin et al., 2007; Schenk et al., 2007). Meanwhile, similar approaches showed that TREM-2 activation generally antagonized activation signals for inflammation (Daws et al., 2001; Colonna, 2003; Hamerman et al., 2006; Turnbull et al., 2006). In contrast, the present results provide for a paradigm in which TREM-2 activation promotes the development of chronic inflammatory disease. This model is consistent with reports for up-regulation of M2 gene expression (including *TREM2*) in macrophages isolated from cigarette smokers with and without COPD (Shaykhiev et al., 2009; Koth et al., 2010). However, these previous studies as well as others that assess association with disease cannot determine cause and effect actions of TREM signaling in the development of disease. Moreover, the present application of new tools to separately study both TREM-1 and TREM-2 deficiency in vivo and in vitro in the same model system was critical to dissect any differences in TREM family member function.

A second unexpected aspect of the present findings is the biological activity of sTREM-2. In fact, we initially approached the issue of TREM-2 activity as being a function of TREM-2 localization to the cell surface, where it could presumably bind to an as yet poorly defined ligand, and in association with DAP12, initiate a signaling pathway for cell survival (Otero et al., 2009). Indeed, we were able to secure evidence for this mechanism in the setting of acute infection, wherein viral replication increases TREM-2 on the surface of infected macrophages. However, this relatively transient effect on macrophage survival did not appear to explain the long-term effect of TREM-2 on postviral lung disease. We therefore pursued evidence that the greatest increases in TREM-2 lung

levels were found long after clearance of infectious virus and were manifest as marked increases in sTREM-2 that had been cleaved from the cell surface. These circumstances led to the unexpected function of sTREM-2 as a potent antiapoptotic factor for macrophages. Our data suggests that sTREM-2 acts as an intracellular messenger to trigger the activation of kinases (e.g., ERK1/2) that promote cell survival. However, additional work will need to define the precise molecular pathway downstream of sTREM-2 actions, including those proposed for TREM-2–DAP12 signaling for cell survival (Otero et al., 2009, 2012). Meanwhile, however, our results may also help to explain the proposed benefit of sTREM-2 cleavage in neurodegenerative disease, where decreased sTREM-2 cleavage caused by mutation may be associated with impaired macrophage (i.e., microglial) function in the CNS (Kleinberger et al., 2014).

A third unanticipated result of our study was the potent role of DAP12 and IL-13 in regulating TREM-2 cleavage and sTREM-2 formation. Similar to signaling function of cell surface TREM-2, the formation of sTREM-2 and any consequent downstream action of sTREM-2 was still dependent on DAP12. This new connection between sTREM-2 and DAP12 could help explain how distinct TREM signals are transduced into different downstream effects on cell behavior. Thus, both TREM-1 and TREM-2 on the cell surface are proposed to signal via DAP12, and this adaptor has only a single immunoreceptor tyrosine-based activation motif (ITAM) for subsequent signal transduction. It has been proposed that the avidity of TREM (or other receptor) interaction with DAP12 might dictate a positive versus negative signal from this ITAM to the downstream kinase (Turnbull and Colonna, 2007). In the present experiments, we find that TREM-2 function is linked to DAP12 by a protein maturation process that appears distinct from TREM-1–DAP12 and TREM-2–DAP12 signaling. Similarly, IL-13 also contributed to the TREM-2 cleavage process in what appears to be a novel role for IL-13. In both cases, additional work is needed to define the molecular mechanism for TREM-2 cleavage. This type of

insight could provide a useful target for antiinflammatory therapy by inhibiting cleavage and a consequent excess of sTREM-2 formation.

A fourth issue that is distinct for our results relates to the view of M2 macrophages and macrophage subsets in mediating inflammatory disease. For example, other disease models such as allergen challenge concentrate on blocking the macrophage response to IL-13 and conclude that there is no role for M2 macrophages in the disease process (Nieuwenhuizen et al., 2012). In contrast, our model focuses on the role of macrophages in IL-13 production as the fundamental step in producing disease, so it is this step that needs to be targeted for disruption. Notably, however, allergen-challenge models may depend on recruited monocytes but not resident alveolar macrophages for the development of lung disease (Zasłona et al., 2014). Similarly, we found differences in tissue monocyte and interstitial macrophage versus alveolar macrophage characteristics (e.g., level of *Il13* mRNA induction and sensitivity to TREM-2 regulation) during the development of postviral disease. These results also support the paradigm of inflammatory monocyte recruitment and subsequent differentiation into disease–producing macrophages and provide a basis for assessing these events in situ with reporter labeling and intravital imaging in the future.

Our study focused on the role of TREM-2 in macrophage function based on evidence that macrophages are key to the development of postviral disease. However, we recognize that myeloid (conventional) DCs may contribute to postviral disease at least in the first few weeks after viral inoculation (Grayson et al., 2007) and may express TREM-2 at least in vitro (Bouchon et al., 2001b; Ito and Hamerman, 2012). We found TREM-2 expression on CD11b⁺CD11c⁻ cells (i.e., monocytes and macrophages) and not on CD11b⁺CD11c⁺ cells (i.e., DCs) at 5 dpi with virus using FACS, but we cannot yet exclude expression on DCs at 49 dpi given the low levels of cellular expression of TREM-2 and the low numbers of DCs at this later time point. Thus, further studies with different technologies will be needed to determine any role for DC-expressed TREM-2 after viral infection.

In sum, we have defined a novel role for TREM-2 in the development of chronic lung disease using a postviral mouse model of this process. Our previous work led to a new consideration of the role of innate immune activation of macrophages in this type of disease. However, there was little subsequent progress toward further understanding and thereby specifically blocking the macrophage component of postviral disease in experimental models or humans. Herein, we describe an unanticipated mechanism whereby TREM-2 allows for macrophages to accumulate in the lung and thereby amplify disease-promoting IL-13 production. In this setting, TREM-2 appears to affect the chronic disease process without influencing acute viral illness, thereby creating an opportunity to inhibit excessive TREM-2 action without compromising host defense. The findings thereby provide an opportunity to downregulate the type 2 immune response and prevent the development of this type of immune-mediated disease by interrupting

sTREM-2 formation or action. Initial studies already suggest an increase in TREM-2 expression in concert with excess levels of airway mucus and M2 macrophages in human lung disease (Byers and Holtzman, 2011; Byers et al. 2013. International Meeting of the American Thoracic Society. Abstr. A141.). The present findings justify further validation of these observations in humans with chronic lung disease and additional work to correct any abnormalities in TREM-2 action in this type of disease and other diseases that implicate a role for TREM-2 in regulating macrophage survival.

MATERIALS AND METHODS

Mice. WT C57BL/6J mice were obtained from The Jackson Laboratory. The *op/opT* mice were generated as described previously (Abboud et al., 2002) and were provided by N. Ghosh-Choudhury (University of Texas, San Antonio). These mice were crossed to WT mice to generate heterozygous *wt/opT* mice and littermate *wt/wt* control mice. *Dap12⁻/⁻* mice were provided by T. Takai (Tohoku University, Sendai, Japan). *Trem2⁻/⁻* mice were generated as described previously (Turnbull et al., 2006). *Trem1/3⁻/⁻* mice were generated as described previously and were backcrossed to C57BL/6 mice until >99% of the loci were derived from this strain. *Tlr3⁻/⁻* mice were generated as described previously (Alexopoulou et al., 2001). *Pkr⁻/⁻* mice were generated as described previously (Yang et al., 1995) and rederived from frozen embryos obtained from M. White and H. Virgin IV (Washington University, St. Louis, MO). All mice were maintained on a C57BL/6 genetic background and were used in protocols approved by Animal Studies Committee of Washington University School of Medicine in accordance with National Institutes of Health guidelines.

Viral inoculation and monitoring. Mice were inoculated with SeV (10⁵ pfu), an equivalent amount of UV-inactivated SeV (SeV-UV), or PBS as described previously (Kim et al., 2008). SeV-UV and PBS inoculations gave identical results, and therefore are treated interchangeably as controls. Viral titers for stock solutions and lung infections were monitored by plaque-forming and real-time PCR assays as described previously (Kim et al., 2008).

Analysis of mRNA. For gene expression microarrays, RNA was isolated and analyzed using Illumina Mouse-WG6 v2 BeadChips (Illumina) as described previously (Byers et al., 2013). Visualization and plotting was performed using DecisionSite for Functional Genomics (TIBCO Spotfire). Microarray data were deposited in the National Center for Biotechnology Information (NCBI) Gene Expression Omnibus (GEO) under series accession nos. GSE49603 and GSE61437. For real-time qPCR assays, RNA was purified from lung homogenate using TRIzol (Invitrogen) and was converted to cDNA using the High-Capacity cDNA Archive kit (Applied Biosystems). Target mRNA was quantified by real-time PCR assay using specific fluorogenic probes and primer sets and the Fast Universal PCR Master Mix system (Applied Biosystems). Primer–probe sets for mouse *Ccl2* (*Mcp-1*; Mm00441242_m1), *Cx3cr1l* (Mm00436454_m1), *Trem1* (Mm00451738_m1), *Trem2* (Mm00451744_m1), *Chi3l3* (Mm00657889_mH), *Arg1* (Mm00475988_m1), and *Dap12* (Mm00449152_m1) were obtained from Applied Biosystems. The forward and reverse primers and probes for mouse *Il13* were 5′-GGTGCCAAGATCTGTGTCTC-3′, 5′-CCACACTCCATACCAT-GCTG-3′, and 5′-AAGACCAGACTCCCCTGTGCAAC-3′; for *Muc5ac* were 5′-TACCACTCCCTGCTTCTGCAGCGTGTCA-3′, 5′-ATAG-TAACAGTGGCCATCAAGGTCTGTCT-3′, and 5′-TATACCCCT-TGGGATCCATCATCTACA-3′; for *Csf1* were 5′-CTTCATGCCA-GATTGCCTTTG-3′, 5′-CGCATGGTCTCATCTATTATGTCT-3′, 5′-CAGCTGGATGATCCTGTTTGCTACCT-3′; and for mouse *Gapdh* were 5′-AAGGTGAAGGTCGGAGTCA-3′, 5′-CATGTAAACCATG-TAGTTGAGGT-3′, and 5′-CGGATTTGGTCGTATTGGGCGC-3′. All

probes were designed to span introns and did not react with genomic DNA. Samples were assayed on the 7500 Fast Real-Time PCR System and analyzed using the 7500 Fast System Software (Applied Biosystems). Levels of specific gene expression were normalized to *Gapdh* mRNA levels.

Western blotting. For TREM-2 expression, BMDMs were seeded in 6-well tissue culture plates and were infected with SeV at MOI 1 and 10 for 48 h. For caspase-3 expression, BMDMs were seeded in 6-well tissue culture plates and were cultured in the presence or absence of L cell-conditioned medium for 16 h. Cells were lysed and boiled in reducing SDS-PAGE sample buffer containing 100 mM Tris, pH 6.8, 4% SDS, 5% β–mercaptoethanol, 20% glycerol and 0.2% bromophenol blue. Lysates was subjected to 4–15% gradient gel electrophoresis (Bio-Rad Laboratories) and transferred to PVDF membrane (Millipore) in 10% methanol, 25 mM Tris and 192 mM glycine, pH 8.3. Anti-Caspase-3 Ab was from Cell Signaling Technology. Rat anti–mouse TREM-2 mAb (clone 178.9.4) was generated as described previously (Turnbull et al., 2006). Antibody binding was detected using the enhanced chemiluminescence (ECL) system (GE Healthcare). Molecular weight standards were run on each blot to validate that each of the indicated bands corresponded to the appropriate molecular weight.

Recombinant protein expression and purification. The mouse TREM-2 Ig domain (amino acid residues 19–136) tagged with 6X His (sTREM-2-his) was expressed, secreted, and purified from mammalian cell culture as previously described (Kober et al., 2014). Precautions were taken to prevent introduction of endotoxin either by using either new, sterile plasticware or by soaking glassware overnight in 0.5 M NaOH. The final purified protein was exchanged in PBS using a microconcentrator (Sartorius). For heat inactivation, sTREM-2-his was boiled at 100°C for 1 h.

Microscopy. Tissues were fixed with 10% formalin, embedded in paraffin, cut into 5-μm sections, and adhered to charged slides. Sections were deparaffinized in Citrosolv (Fisherbrand), hydrated, and in the case of immunofluorescence microscopy, treated with heat-activated antigen unmasking solution (Vector Laboratories). Immunostaining of mouse tissue was performed using anti-MUC5AC mAb (Thermo Fisher Scientific; clone 45M1), anti–Mac-3 mAb (BD; clone M3/84), anti–Caspase-3 mAb (clone 5A1E; Cell Signaling Technology), anti–mouse TREM-2 (R&D Systems), anti–mouse F4/80 mAb (clone CI:A3-1; Abcam), anti–mouse phospho-ERK1/2 (clone D13.14.4E, Cell Signaling Technology), anti–mouse IL-13 mAb (R&D Systems), and anti-SeV antibody (SPAFAS, Inc.). Antibody binding was visualized using Alexa Fluor 488 or 594 fluorochromes (Invitrogen). Slides were counterstained with DAPI-containing mounting media (Vector Laboratories).

For sTREM-2 immunostaining, BMDMs were seeded into 2-well chamber slide (Nalge Nunc International) at 2×10^5 cell per well. For surface sTREM-2 immunostaining, BMDMs were incubated with sTREM2-his (10 μg/ml) for 30 min on ice and then washed four times with chilled PBS and incubated with mouse anti-6X His tag antibody (Abcam; clone His. H8) followed by Alexa Fluor 488–conjugated anti–mouse IgG (Invitrogen) and fixation with 4% PFA. For intracellular sTREM-2 immunostaining, cells were incubated with sTREM-2-his for 30 min at 37°C, washed with PBS, fixed with 4% PFA, and then permeabilized with 0.2% Saponin, 2% BSA in PBS for 30 min before incubation with anti-6X His tag antibody and Alexa Fluor 488–conjugated anti–mouse IgG. All microscopy was performed using an Olympus BX51 microscope and a Retiga-2000R camera system (QImaging).

Flow cytometry and FACS. Single-cell lung suspensions were made from minced lung tissue subjected to collagenase (Liberase Blendzyme III; Roche), hyaluronidase (Sigma-Aldrich), and DNase I (grade II; Roche) digestion for 45 min at 37°C and then treated with ACK buffer to remove red blood cells. Cell percentages were unchanged if lungs were perfused before digestion (suggesting that intravascular cells did not contribute significantly to the analysis), so unperfused lungs were used for all experiments. Staining of surface markers was performed using FcR blockade and fluorochrome-conjugated

mAb at 4°C. We used the following antibodies: rat anti-mCD11b (clone M1/70; eBioscience), anti-Ly6C (clone al-21; BD), anti-Ly6G (clone 1a8; BD), anti-mouse F4/80 (clone BM8; eBioscience), anti-mouse TREM-1 (clone 174031; R&D Systems), anti-m/hTREM-2 (clone 237920; R&D Systems), anti–mouse CD11c (clone HL3; BD), anti–mouse CD45.2 (clone 104; eBioscience), and anti–mouse Siglec-F (clone E50-2440; BD). We used flow cytometry and FACS to identify and purify specific cell populations in mouse lungs using the following gates: tissue monocytes as SSC^{low}Ly6G$^-$F4/80$^+$CD11b$^+$, interstitial macrophages as SSC^{high}CD11c$^-$Ly6G$^-$Siglec-F$^-$F4/80$^+$CD11b$^+$, alveolar macrophages as SSC^{high}CD11c$^+$Ly6G$^-$Siglec-F$^+$F4/80$^+$CD11b$^-$, and neutrophil gate as SSC^{high}Ly6G$^+$ (Fig. S1). Analysis was performed using Moflo (DAKO-Cytomation) and FlowJo software (Tree Star). Cells were counted using flow cytometry and fluorescent counting beads (CountBright; Life Technologies).

Cell culture. Bone marrow cells were flushed from femurs and differentiated in 150×15 mm Petri dishes in DMEM medium containing 0.29 g/liter L-glutamine, 1 mM sodium pyruvate, 10% FBS, and 30% L929 fibroblast-conditioned medium as a source of CSF-1. At day 6 or indicated times, BMDMs were resuspended by incubation in 1 mM EDTA in PBS for 10 min on ice, washed twice with PBS and plated into tissue culture plates. In some experiments, BMDMs were incubated with poly(IC) (Sigma-Aldrich) or mouse IL-13 (R&D Systems). For cell viability assays, BMDMs were seeded into 96-well tissue culture plates at 5×10^4 cells per well and were assessed for viability using the Cell Proliferation kit (XTT) from Roche. For cell proliferation assays, BMDMs were seeded into 6-well tissue culture plates, labeled for 18 h with BrdU (10 μM), and then assessed using flow cytometry with the FITC BrdU Flow kit (BD).

Apoptosis assays. For propidium iodide (PI) assay, BMDMs were cultured in L cell–conditioned medium for 5 d and deprived of CSF-1 for 1 d to induce apoptosis (Otero et al., 2009). Cells were detached using EDTA (1 mM) in PBS, washed, fixed with 70% ethanol, and incubated with PI (50 μg/ml) and RNase (40 μg/ml) for 1 h. Samples were analyzed for DNA content using a FACScan (BD). For Annexin V assay, BMDMs were differentiated in L cell–conditioned medium for 5 d, detached with EDTA, seeded onto the poly-D-Lysine-coated coverslips (BD) placed in a 24-well plate, and cultured in medium without CSF-1 for 1 d. PI and Annexin V immunostaining was performed according to the manufacture's protocol (Invitrogen). Annexin V–positive, PI-negative staining cells were quantified using microscopy, and values were expressed as the percentage of apoptotic cells (Annexin V positive, PI negative) relative to the total number of cells in 6 randomly selected fields of the two wells.

Monocyte influx. For analysis of monocyte influx into the lung, BMMs were purified from CD45.2 WT and *Trem2$^{-/-}$* mice using negative selection with the EasySep Mouse Monocyte Enrichment kit (StemCell Technologies). Purified monocytes were then introduced into CD45.1 WT mice (3×10^6 cells per mouse via tail vein injection) at 0 dpi with SeV, and the number of CD45.2$^+$ cells in the lung was determined 3 or 5 d later using FACS and fluorescent counting beads.

ELISA. For lung tissue samples, lung tissue was minced and then homogenized in PBS containing protease inhibitor cocktail (cOmplete; Roche) using a rotor-type homogenizer (Tissue-Tearor; Biospec Products). For cell supernatant and lysate samples, BMDM (2×10^6 cells in 2 ml of complete DMEM containing 15% L cell–conditioned medium) were seeded into 12-well tissue plates, treated with or without IL-13 (20 ng/ml) or SeV (MOI 1 and 10). Cell supernatants were collected, and cells were washed twice with chilled PBS and then lysed in radio-immunoprecipitation assay (RIPA) buffer (Sigma-Aldrich) containing protease inhibitors. Levels of CSF-1 were determined using a Duoset ELISA kit (R&D Systems) and levels of cellular TREM-2 and sTREM-2 with a TREM-2 ELISA kit (Antibodies-online.com).

Statistical analyses. For experiments in mice and cell culture, all experiments were repeated a minimum of three times, and representative values are presented. PCR data were presented as mean ± SEM and was analyzed using an unpaired Student's *t* test. If variances were unequal, Welch's correction was applied. For all analyses, P < 0.05 were considered significant. For SeV-GFP versus TREM-2 expression, nonlinear curve fit was performed using a simple hyperbolic function where $Y = B_{max} \times X/(K_d + X)$.

Online supplemental material. Fig. S1 shows the flow cytometry scheme for analysis of lung macrophages. Fig. S2 shows a scheme for FACS analysis of cell surface and intracellular TREM-2 immunostaining. Table S1 shows microarray gene expression values for Fig. 2 A, including values for all TREM family members. Online supplemental material is available at http://www.jem.org/cgi/content/full/jem.20141732/DC1.

REFERENCES

Abboud, S.L., K. Woodruff, C. Liu, V. Shen, and N. Ghosh-Choudhury. 2002. Rescue of the osteopetrotic defect in op/op mice by osteoblast-specific targeting of soluble colony-stimulating factor-1. *Endocrinology.* 143:1942–1949. http://dx.doi.org/10.1210/endo.143.5.8775

Agapov, E., J.T. Battaile, R. Tidwell, R. Hachem, G.A. Patterson, R.A. Pierce, J.J. Atkinson, and M.J. Holtzman. 2009. Macrophage chitinase 1 stratifies chronic obstructive lung disease. *Am. J. Respir. Cell Mol. Biol.* 41:379–384. http://dx.doi.org/10.1165/2009-0122R

Alevy, Y.G., A.C. Patel, A.G. Romero, D.A. Patel, J. Tucker, W.T. Roswit, C.A. Miller, R.F. Heier, D.E. Byers, T.J. Brett, and M.J. Holtzman. 2012. IL-13-induced airway mucus production is attenuated by MAPK13 inhibition. *J. Clin. Invest.* 122:4555–4568. http://dx.doi.org/10.1172/JCI64896

Alexopoulou, L., A.C. Holt, R. Medzhitov, and R.A. Flavell. 2001. Recognition of double-stranded RNA and activation of NF-kappaB by Toll-like receptor 3. *Nature.* 413:732–738. http://dx.doi.org/10.1038/35099560

Bleharski, J.R., V. Kiessler, C. Buonsanti, P.A. Sieling, S. Stenger, M. Colonna, and R.L. Modlin. 2003. A role for triggering receptor expressed on myeloid cells-1 in host defense during the early-induced and adaptive phases of the immune response. *J. Immunol.* 170:3812–3818. http://dx.doi.org/10.4049/jimmunol.170.7.3812

Bouchon, A., J. Dietrich, and M. Colonna. 2000. Cutting edge: inflammatory responses can be triggered by TREM-1, a novel receptor expressed on neutrophils and monocytes. *J. Immunol.* 164:4991–4995. http://dx.doi.org/10.4049/jimmunol.164.10.4991

Bouchon, A., F. Facchetti, M.A. Weigand, and M. Colonna. 2001a. TREM-1 amplifies inflammation and is a crucial mediator of septic shock. *Nature.* 410:1103–1107. http://dx.doi.org/10.1038/35074114

Bouchon, A., C. Hernández-Munain, M. Cella, and M. Colonna. 2001b. A DAP12-mediated pathway regulates expression of CC chemokine receptor 7 and maturation of human dendritic cells. *J. Exp. Med.* 194:1111–1122. http://dx.doi.org/10.1084/jem.194.8.1111

Byers, D.E., and M.J. Holtzman. 2011. Alternatively activated macrophages and airway disease. *Chest.* 140:768–774. http://dx.doi.org/10.1378/chest.10-2132

Byers, D.E., J. Alexander-Brett, A.C. Patel, E. Agapov, G. Dang-Vu, X. Jin, K. Wu, Y. You, Y. Alevy, J.-P. Girard, et al. 2013. Long-term

IL-33-producing epithelial progenitor cells in chronic obstructive lung disease. *J. Clin. Invest.* 123:3967–3982. http://dx.doi.org/10.1172/JCI65570

Colonna, M. 2003. TREMs in the immune system and beyond. *Nat. Rev. Immunol.* 3:445–453. http://dx.doi.org/10.1038/nri1106

Daws, M.R., L.L. Lanier, W.E. Seaman, and J.C. Ryan. 2001. Cloning and characterization of a novel mouse myeloid DAP12-associated receptor family. *Eur. J. Immunol.* 31:783–791. http://dx.doi.org/10.1002/1521-4141(200103)31:3<783::AID-IMMU783>3.0.CO;2-U

Fortin, C.F., O. Lesur, and T. Fulop Jr. 2007. Effects of TREM-1 activation in human neutrophils: activation of signaling pathways, recruitment into lipid rafts and association with TLR4. *Int. Immunol.* 19:41–50. http://dx.doi.org/10.1093/intimm/dxl119

Grayson, M.H., D. Cheung, M.M. Rohlfing, R. Kitchens, D.E. Spiegel, J. Tucker, J.T. Battaile, Y. Alevy, L. Yan, E. Agapov, et al. 2007. Induction of high-affinity IgE receptor on lung dendritic cells during viral infection leads to mucous cell metaplasia. *J. Exp. Med.* 204:2759–2769. http://dx.doi.org/10.1084/jem.20070360

Hamerman, J.A., J.R. Jarjoura, M.B. Humphrey, M.C. Nakamura, W.E. Seaman, and L.L. Lanier. 2006. Cutting edge: inhibition of TLR and FcR responses in macrophages by triggering receptor expressed on myeloid cells (TREM)-2 and DAP12. *J. Immunol.* 177:2051–2055. http://dx.doi.org/10.4049/jimmunol.177.4.2051

Holtzman, M.J. 2012. Asthma as a chronic disease of the innate and adaptive immune systems responding to viruses and allergens. *J. Clin. Invest.* 122:2741–2748. http://dx.doi.org/10.1172/JCI60325

Holtzman, M.J., D.E. Byers, J. Alexander-Brett, and X. Wang. 2014. The role of airway epithelial cells and innate immune cells in chronic respiratory disease. *Nat. Rev. Immunol.* 14:686–698. http://dx.doi.org/10.1038/nri3739

Ito, H., and J.A. Hamerman. 2012. TREM-2, triggering receptor expressed on myeloid cell-2, negatively regulates TLR responses in dendritic cells. *Eur. J. Immunol.* 42:176–185. http://dx.doi.org/10.1002/eji.201141679

Kaifu, T., J. Nakahara, M. Inui, K. Mishima, T. Momiyama, M. Kaji, A. Sugahara, H. Koito, A. Ujike-Asai, A. Nakamura, et al. 2003. Osteopetrosis and thalamic hypomyelinosis with synaptic degeneration in DAP12-deficient mice. *J. Clin. Invest.* 111:323–332. http://dx.doi.org/10.1172/JCI16923

Kim, E.Y., J.T. Battaile, A.C. Patel, Y. You, E. Agapov, M.H. Grayson, L.A. Benoit, D.E. Byers, Y. Alevy, J. Tucker, et al. 2008. Persistent activation of an innate immune response translates respiratory viral infection into chronic lung disease. *Nat. Med.* 14:633–640. http://dx.doi.org/10.1038/nm1770

Kleinberger, G., Y. Yamanishi, M. Suárez-Calvet, E. Czirr, E. Lohmann, E. Cuyvers, H. Struyfs, N. Pettkus, A. Wenninger-Weinzierl, F. Mazaheri, et al. 2014. TREM2 mutations implicated in neurodegeneration impair cell surface transport and phagocytosis. *Sci. Transl. Med.* 6:243ra86. http://dx.doi.org/10.1126/scitranslmed.3009093

Klesney-Tait, J., K. Keck, X. Li, S. Gilfillan, K. Otero, S. Baruah, D.K. Meyerholz, S.M. Varga, C.J. Knudson, T.O. Moninger, et al. 2013. Transepithelial migration of neutrophils into the lung requires TREM-1. *J. Clin. Invest.* 123:138–149. http://dx.doi.org/10.1172/JCI64181

Kober, D.L., K.M. Wanhainen, B.M. Johnson, D.T. Randolph, M.J. Holtzman, and T.J. Brett. 2014. Preparation, crystallization, and preliminary crystallographic analysis of wild-type and mutant human TREM-2 ectodomains linked to neurodegenerative and inflammatory diseases. *Protein Expr. Purif.* 96:32–38. http://dx.doi.org/10.1016/j.pep.2014.01.015

Koth, L.L., C.J. Cambier, A. Ellwanger, M. Solon, L. Hou, L.L. Lanier, C.L. Abram, J.A. Hamerman, and P.G. Woodruff. 2010. DAP12 is required for macrophage recruitment to the lung in response to cigarette smoke and chemotaxis toward CCL2. *J. Immunol.* 184:6522–6528. http://dx.doi.org/10.4049/jimmunol.0901171

Netea, M.G., T. Azam, G. Ferwerda, S.E. Girardin, S.H. Kim, and C.A. Dinarello. 2006. Triggering receptor expressed on myeloid cells-1 (TREM-1) amplifies the signals induced by the NACHT-LRR (NLR) pattern recognition receptors. *J. Leukoc. Biol.* 80:1454–1461. http://dx.doi.org/10.1189/jlb.1205758

Nieuwenhuizen, N.E., F. Kirstein, J. Jayakumar, B. Emedi, R. Hurdayal, W.G.C. Horsnell, A.L. Lopata, and F. Brombacher. 2012. Allergic airway disease is unaffected by the absence of IL-4Rα-dependent alternatively

activated macrophages. *J. Allergy Clin. Immunol.* 130:743–750: e8. http://dx.doi.org/10.1016/j.jaci.2012.03.011

Otero, K., I.R. Turnbull, P.L. Poliani, W. Vermi, E. Cerutti, T. Aoshi, I. Tassi, T. Takai, S.L. Stanley, M. Miller, et al. 2009. Macrophage colony-stimulating factor induces the proliferation and survival of macrophages via a pathway involving DAP12 and beta-catenin. *Nat. Immunol.* 10:734–743. http://dx.doi.org/10.1038/ni.1744

Otero, K., M. Shinohara, H. Zhao, M. Cella, S. Gilfillan, A. Colucci, R. Faccio, F.P. Ross, S.L. Teitelbaum, H. Takayanagi, and M. Colonna. 2012. TREM2 and β-catenin regulate bone homeostasis by controlling the rate of osteoclastogenesis. *J. Immunol.* 188:2612–2621. http://dx.doi.org/10.4049/jimmunol.1102836

Schenk, M., A. Bouchon, F. Seibold, and C. Mueller. 2007. TREM-1–expressing intestinal macrophages crucially amplify chronic inflammation in experimental colitis and inflammatory bowel diseases. *J. Clin. Invest.* 117:3097–3106. http://dx.doi.org/10.1172/JCI30602

Seno, H., H. Miyoshi, S.L. Brown, M.J. Geske, M. Colonna, and T.S. Stappenbeck. 2009. Efficient colonic mucosal wound repair requires Trem2 signaling. *Proc. Natl. Acad. Sci. USA.* 106:256–261. http://dx.doi.org/10.1073/pnas.0803343106

Shaykhiev, R., A. Krause, J. Salit, Y. Strulovici-Barel, B.G. Harvey, T.P. O'Connor, and R.G. Crystal. 2009. Smoking-dependent reprogramming of alveolar macrophage polarization: implication for pathogenesis of chronic obstructive pulmonary disease. *J. Immunol.* 183:2867–2883. http://dx.doi.org/10.4049/jimmunol.0900473

Takahashi, K., M. Prinz, M. Stagi, O. Chechneva, and H. Neumann. 2007. TREM2-transduced myeloid precursors mediate nervous tissue debris clearance and facilitate recovery in an animal model of multiple sclerosis. *PLoS Med.* 4:e124. http://dx.doi.org/10.1371/journal.pmed.0040124

Turnbull, I.R., and M. Colonna. 2007. Activating and inhibitory functions of DAP12. *Nat. Rev. Immunol.* 7:155–161. http://dx.doi.org/10.1038/nri2014

Turnbull, I.R., S. Gilfillan, M. Cella, T. Aoshi, M. Miller, L. Piccio, M. Hernandez, and M. Colonna. 2006. Cutting edge: TREM-2 attenuates macrophage activation. *J. Immunol.* 177:3520–3524. http://dx.doi.org/10.4049/jimmunol.177.6.3520

Tyner, J.W., O. Uchida, N. Kajiwara, E.Y. Kim, A.C. Patel, M.P. O'Sullivan, M.J. Walter, R.A. Schwendener, D.N. Cook, T.M. Danoff, and M.J. Holtzman. 2005. CCL5-CCR5 interaction provides antiapoptotic signals for macrophage survival during viral infection. *Nat. Med.* 11:1180–1187. http://dx.doi.org/10.1038/nm1303

Tyner, J.W., E.Y. Kim, K. Ide, M.R. Pelletier, W.T. Roswit, J.D. Morton, J.T. Battaile, A.C. Patel, G.A. Patterson, M. Castro, et al. 2006. Blocking airway mucous cell metaplasia by inhibiting EGFR antiapoptosis and IL-13 transdifferentiation signals. *J. Clin. Invest.* 116:309–321. http://dx.doi.org/10.1172/JCI25167

Walter, M.J., J.D. Morton, N. Kajiwara, E. Agapov, and M.J. Holtzman. 2002. Viral induction of a chronic asthma phenotype and genetic segregation from the acute response. *J. Clin. Invest.* 110:165–175. http://dx.doi.org/10.1172/JCI0214345

Yang, Y.L., L.F.L. Reis, J. Pavlovic, A. Aguzzi, R. Schäfer, A. Kumar, B.R. Williams, M. Aguet, and C. Weissmann. 1995. Deficient signaling in mice devoid of double-stranded RNA-dependent protein kinase. *EMBO J.* 14:6095–6106.

Zasłona, Z., S. Przybranowski, C. Wilke, N. van Rooijen, S. Teitz-Tennenbaum, J.J. Osterholzer, J.E. Wilkinson, B.B. Moore, and M. Peters-Golden. 2014. Resident alveolar macrophages suppress, whereas recruited monocytes promote, allergic lung inflammation in murine models of asthma. *J. Immunol.* 193:4245–4253. http://dx.doi.org/10.4049/jimmunol.1400580